Hindawi Publishing Corporation
Journal of Nanomaterials
Volume 2015, Article ID 258342, 6 pages
http://dx.doi.org/10.1155/2015/258342

Research Article

Synthesis and Characterization of High Efficiency and Stable Spherical Ag_3PO_4 Visible Light Photocatalyst for the Degradation of Methylene Blue Solutions

Liqin Qin,[1] Pingfang Tao,[1] Xiaosong Zhou,[2] Qi Pang,[3] Chunjie Liang,[1] Kuo Liu,[1] and Xujian Luo[1]

[1]*Guangxi Key Laboratory of Farm Products Processing (Cultivation Base), Colleges and Universities Key Laboratory for Efficient Use of Agricultural Resources in the Southeast of Guangxi, College of Chemistry and Material, Yulin Normal University, Yulin, Guangxi 537000, China*
[2]*School of Chemistry and Chemical Engineering and Institute of Physical Chemistry, Lingnan Normal University, Zhanjiang 524048, China*
[3]*School of Chemistry and Chemical Engineering, Guangxi University, Nanning, Guangxi 530004, China*

Correspondence should be addressed to Xiaosong Zhou; zxs801213@163.com

Received 26 November 2014; Revised 28 January 2015; Accepted 29 January 2015

Academic Editor: Stefano Bellucci

A facile method for the synthesis of Ag_3PO_4 visible light photocatalyst has been developed to improve the photocatalytic activity and stability. The as-prepared samples are investigated by X-ray powder diffraction, scanning electron microscopy, infrared spectroscopy, photoluminescence (PL) spectroscopy, and UV-Vis diffuse reflectance spectroscopy techniques. The results reveal that the prepared Ag_3PO_4 has cube structure with a band gap of 2.26 eV. The as-prepared samples show higher photocatalytic activity for methylene blue (MB) degradation than that of N-TiO_2 under visible light irradiation.

1. Introduction

Semiconductor based photocatalysts have received great attention due to their applications in environmental pollution mediation and solar energy conversion [1–6]. However, the major challenge in the practical applications is their poor efficiency in visible light range or insufficient charge separation ability. To resolve this problem, significant efforts have been devoted to the exploration and fabrication of novel photocatalytic materials for improving photocatalytic properties [7, 8]. To address this issue, diverse techniques in recent years have been focused on the exploration and fabrication of novel semiconductor catalysts to improve photocatalytic properties [9–11]. Recently, Bi and coworkers have reported the new use of a Ag_3PO_4 semiconductor in photocatalytic applications, which exhibits extremely high photooxidative capabilities for O_2 evolution from water as well as organic dyes decomposition under visible light irradiation [12, 13]. Otherwise, this novel photocatalyst can achieve quantum efficiency up to 90% at wavelengths longer than 420 nm, significantly higher than previously reported values. Interestingly, they have further studied the facet effect on photocatalytic performances based on single-crystalline Ag_3PO_4 rhombic dodecahedrons exposed with {110} planes and cubes bound by {100} planes [14]. Unfortunately, Ag_3PO_4 nanoparticles suffer from stability issues in practical applications because they can photochemically decompose if no sacrificial reagent is involved. Furthermore, the consumption of a large amount of noble metal, silver, strongly limits its practical environmental applications. So it remains a great challenge to develop feasible methods for the synthesis of well-defined hierarchical Ag_3PO_4 nanoparticles.

Herein, we successfully fabricated spherical Ag_3PO_4 submicron particles by a simple hydrothermal method. The as-prepared samples were characterized and used for photocatalytic degradation of MB under visible light irradiation.

2. Experimental

In a typical experiment, using CH_3COOAg and K_2HPO_4 as starting materials, (A) 0.50 g of CH_3COOAg (0.003 mol) is dissolved in 20 mL of deionized water and stirred for 10 minutes, and the solution pH adjusts to 9 with ammonia. (B) 0.1742 g of K_2HPO_4 (0.001 mol) is dissolved in 15 mL of deionized water and stirred for 10 minutes. Then solution (B) is added dropwise to solution (A) with stirring. After the resulting solution is magnetically stirred for 30 minutes, the suspension is transferred into a 50 mL Teflon-lined stainless-steel autoclave and heated at 120°C for 24 h. After being cooled naturally to room temperature, the products are collected by centrifugation, washed with deionized water and absolute ethanol several times, and dried under vacuum at 60°C for 24 h. The as-synthesized samples are denoted as Ag_3PO_4-120.

As a comparison, a precipitation method is used to prepare to Ag_3PO_4. 0.50 g of CH_3COOAg (0.003 mol) is dissolved in the beaker with 20 mL of deionized water and magnetically stirred for 10 minutes, then 0.1742 g of K_2HPO_4 (0.001 mol) and 0.5182 g $C_6H_5Na_3O_7{\cdot}2H_2O$ (0.002 mol) are added to the solution. The solution pH adjusts to 5 with HNO_3 (0.01 M). The suspension is stirred for 6 h at room temperature. The products are collected by centrifugation, washed with deionized water and absolute ethanol several times, and dried under vacuum at 60°C for 24 h. The as-synthesized samples are denoted as Ag_3PO_4-P.

X-ray diffraction (XRD) patterns were recorded on an X-ray diffractometer (Bruker D8-Advance, Germany) using Cu Ka radiation. The surface morphology was examined by a scanning electron microscopy (SEM, Quanta 250, FEI Company). UV-Vis diffuse reflectance spectra (DRS) were recorded with a UV-Vis spectrophotometer by using $BaSO_4$ as the reference (UV-2500, Shimadzu). The Fourier transform infrared (FTIR) spectrum was recorded with a GX spectrophotometer (Spectrum 100, Perkin-Elmer) with the KBr wafer technique. The photoluminescence (PL) spectrum was conducted on a Hitachi F-2500 fluorescence spectroscope.

The photocatalytic reaction was conducted in a 200 mL cylindrical glass vessel fixed in the XPA-II photochemical reactor. A 500 W Xe lamp was used as the simulated solar light source (UV-visible light), and a house-made filter was mounted on the lamp to eliminate infrared irradiation. The visible-light was obtained by using the cut-off filter. The cut-off filter was made up of 1 M sodium nitrite solution which can absorb the light with wavelength under 400 nm [15, 16]. This solution was injected into the interlayer of the quartz cool trap and was placed behind the water filter to completely remove the UV portion of the radiation and to supply a visible-light source. MB with the concentration of 20 mg/L was used as contamination. In order to obtain an optimally dispersed system and reach complete adsorption/desorption equilibration, 20 mg photocatalyst powder dispersed in 200 mL reaction solutions by supersonic for 15 min and then the suspension was magnetically stirred in dark for 1 h. During the photocatalytic reaction, air was blown into the reaction medium at a flow rate of 200 mL/min. At regular intervals, 8 mL of the suspension was filtered and then centrifuged. The concentration of the remaining MB was measured by its absorbance (A) at 664 nm with a Hitachi UV-2550 spectrophotometer. The degradation ratio of MB can be calculated by $X = (A_0 - A)/A_0 \times 100\%$.

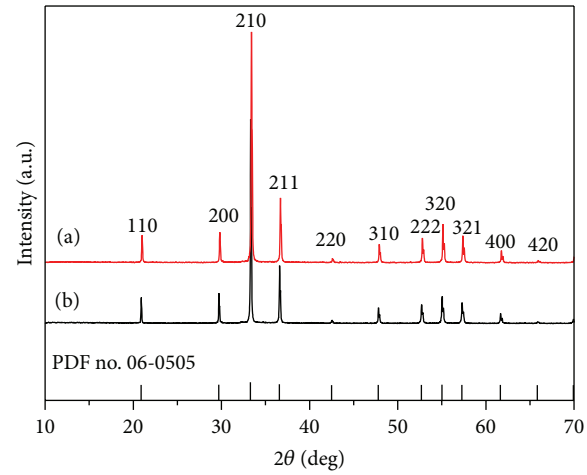

Figure 1: XRD patterns of the as-prepared samples: (a) Ag_3PO_4-120; (b) Ag_3PO_4-P.

3. Results and Discussion

3.1. SEM and XRD Analyses of the As-Synthesized Samples. The XRD patterns of the as-prepared samples synthesized by different methods are shown in Figure 1. It is clear to see that all of the diffraction peaks of Ag_3PO_4-120 corresponded to the cubic phase of Ag_3PO_4 (JCPDS number 06-0505) [14], as well as the characteristic diffraction peaks (110), (200), (210), (211), (220), (310), (222), (320), (321), (400), and (420) (Figure 1(a)). The crystal type of Ag_3PO_4-P is the same as that of Ag_3PO_4-120. It is noted that the as-prepared samples are all of the cubic phase of Ag_3PO_4.

Figure 2 shows the typical SEM images of Ag_3PO_4 products synthesized by different reacting temperatures of hydrothermal method. It can be truly seen that the single-crystalline Ag_3PO_4 submicrocubes with spherical and smooth surfaces have been fabricated in large quantities, and their main diameters range from 500 to 800 nm (Figure 2(a)). With the increase of the reaction temperature, the morphology of crystalline Ag_3PO_4 was unchanged obviously (Figures 2(a)–2(c)). However, the diameters of single-crystalline Ag_3PO_4 are more and more large. Ag_3PO_4-P is irregular oval ball and the main diameters range from 5 μm (Figure 2(d)).

3.2. DRS and IR Analyses of the As-Prepared Samples. Figure 3 shows the UV-Vis absorption spectra of Ag_3PO_4-120, Ag_3PO_4-P, and N-TiO_2. The UV-Vis spectrum of the Ag_3PO_4-120 indicates that it absorbs sunlight with a wavelength less than 548 nm, corresponding to 2.26 eV of band gap energy. This result does not agree with the light-absorption property of Ag_3PO_4 powders reported by another group [17]. This maybe was attributed to the surface plasmon resonance effect

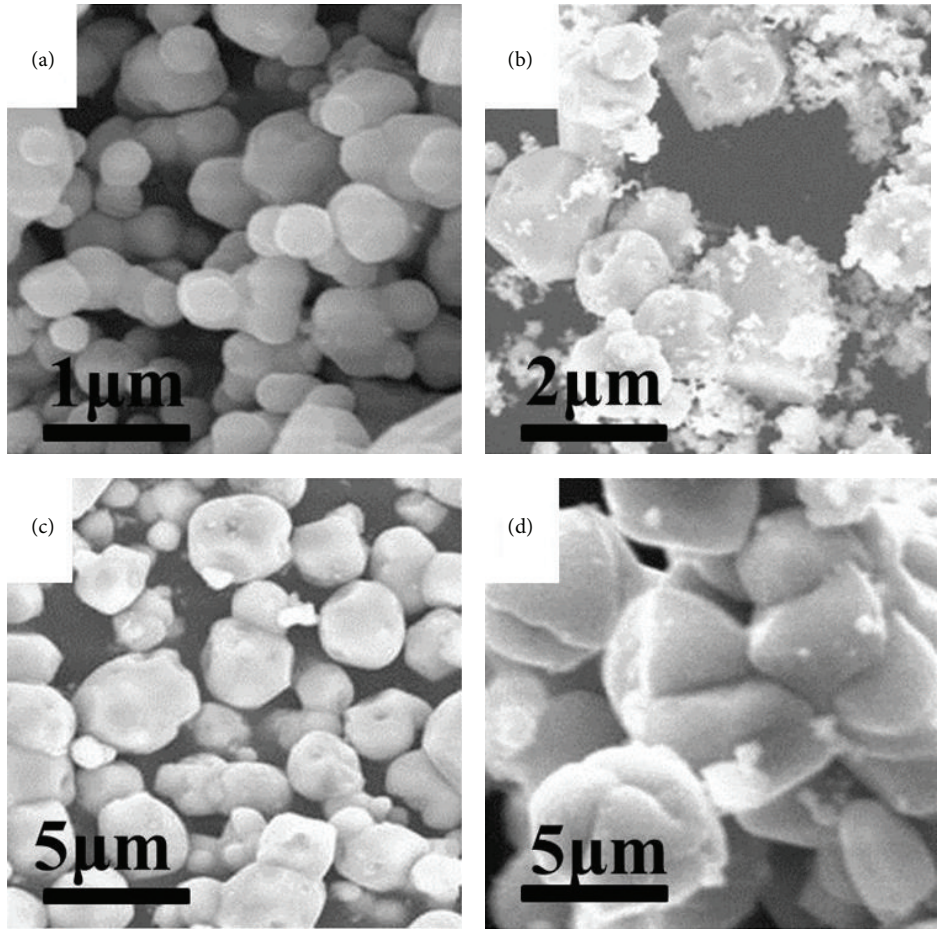

FIGURE 2: SEM of the as-synthesized samples: (a) Ag_3PO_4-120; (b) Ag_3PO_4-140; (c) Ag_3PO_4-160; (d) Ag_3PO_4-P.

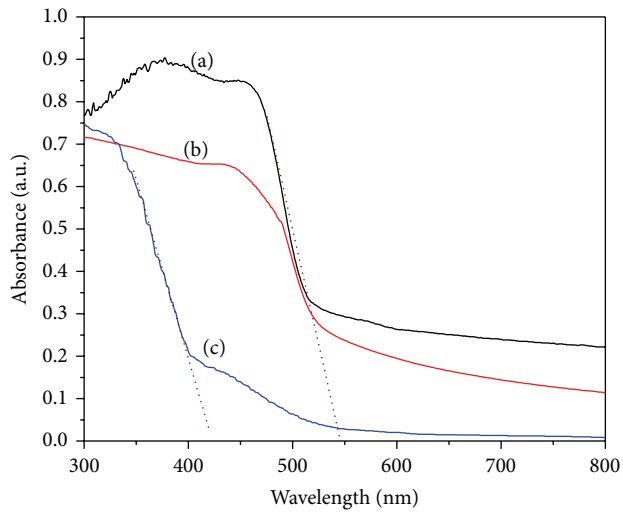

FIGURE 3: UV-Vis spectra of the as-synthesized samples: (a) Ag_3PO_4-P; (b) Ag_3PO_4-120; (c) N-TiO_2.

of the coexistence of silver [18, 19]. However, the absorption band edge of Ag_3PO_4-P is the same as Ag_3PO_4-120; N-TiO_2 appears at 424 nm based on its UV-Vis spectrum, respectively. This feature of UV-Vis light absorption properties of the as-prepared samples suggests that the Ag_3PO_4-120 photocatalyst could be used for visible light photocatalytic reactions.

The IR patterns of the Ag_3PO_4-120, Ag_3PO_4-P are shown in Figure 4. The IR peaks of the samples prepared by hydrothermal and precipitation methods have all appeared in 551 cm^{-1} and 1015 cm^{-1}, which is attributable to the P–O antisymmetric stretching mode of PO_4^{3-}. The IR peak at 846 cm^{-1} may be C–O vibration, which is the impurities of precursor. The peaks appearing at 1399 cm^{-1} and 1655 cm^{-1} are due to torsional vibration H_3O^+. The weak signal of C–H bond is observed at 3230 cm^{-1} [20, 21].

3.3. Photocatalytic Activities of the As-Synthesized Samples. Figure 5 shows the effect of reacting temperature of hydrothermal on the rate of MB degradation under visible light irradiation. The photodegradation efficiency of Ag_3PO_4-120 is 92% after 4 min illumination, but that of Ag_3PO_4-180 is only 35%. After 10 min irradiation, the photodegradation efficiency of Ag_3PO_4-120 can nearly reach 95%; Ag_3PO_4-100 and Ag_3PO_4-160 both reach about 90%. Ag_3PO_4-120 has higher photocatalytic efficiency than other different reacting temperatures of samples. For comparison, the photocatalytic performances of Ag_3PO_4-P and commercial N-doped TiO_2

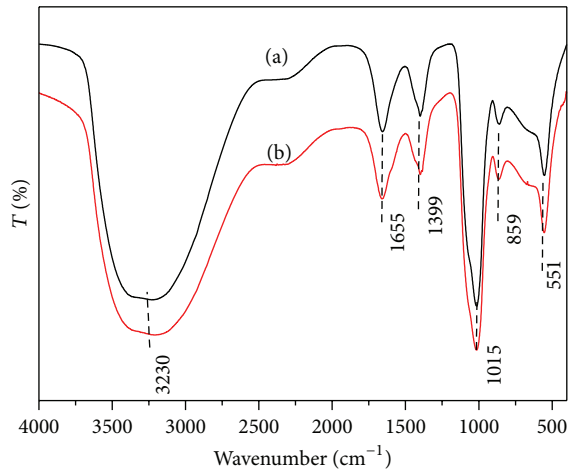

FIGURE 4: IR spectra of the as-synthesized samples: (a) Ag_3PO_4-120; (b) Ag_3PO_4-P.

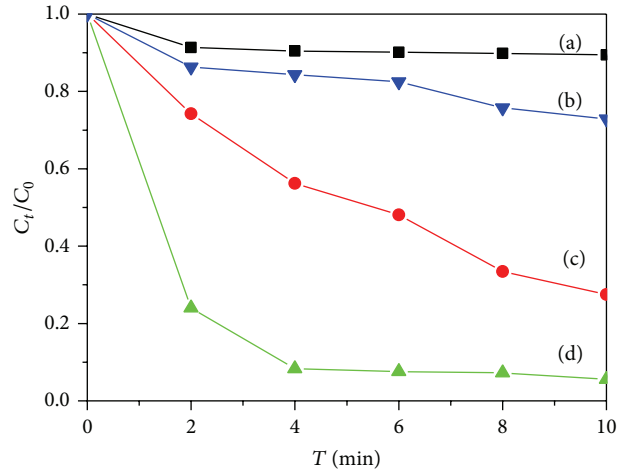

FIGURE 6: Photodegradation plots of MB solution with different catalysts under visible light irradiation: (a) blank; (b) N-TiO_2; (c) Ag_3PO_4-P; (d) Ag_3PO_4-120.

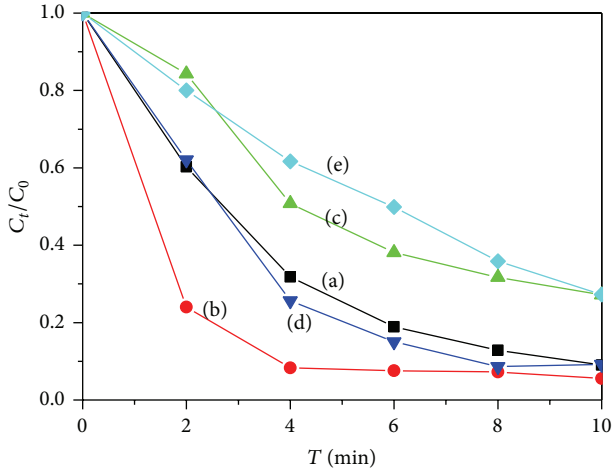

FIGURE 5: Photodegradation plots of MB solution with Ag_3PO_4 obtained at different temperatures: (a) 100°C; (b) 120°C; (c) 140°C; (d) 160°C; (e) 180°C.

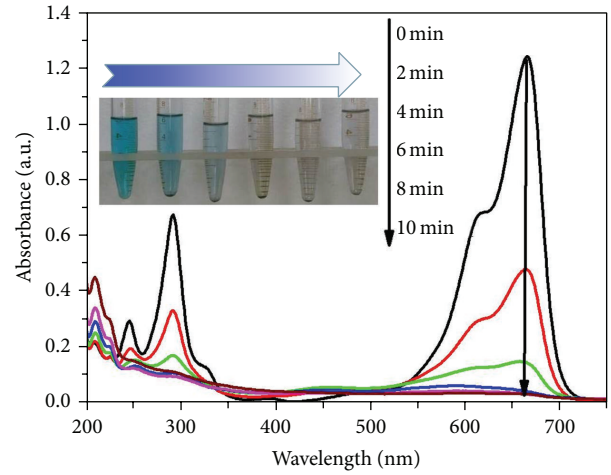

FIGURE 7: UV-Vis absorption spectra of MB solution as a function of irritation time in the presence of Ag_3PO_4-120 (inset shows the corresponding photographs of MB solution).

catalysts have also been studied and compared in Figure 6. As shown in Figure 6, it can be clearly seen that except for N-doped TiO_2 catalysts, all these Ag_3PO_4 samples exhibit excellent photocatalytic activities for the MB degradation. Ag_3PO_4-120 especially exhibits the highest photocatalytic activity, which can nearly completely degrade MB dye in only 4 min. The absorption variation of MB dye over Ag_3PO_4-120 at different irradiation times is shown in Figure 7. The Ag_3PO_4-120 sample needs about 6 min that the MB dye is nearly colorless. At present, we consider that Ag_3PO_4-120 can effectively improve light harvesting as a result of its high surface area. On the other hand, such novel spherical structures could promote the separation of photoexcited carriers and minimize the probability of electron-hole recombination [22]. However, the photocatalytic mechanism over Ag_3PO_4-120 structure cannot be completely understood and a more detailed study is still needed.

As reusability of photocatalyst is a key issue for practical application, Figure 8 shows that the reusability of Ag_3PO_4-120 for degradation of MB under visible light irradiation. As no obvious decrease of degradation is observed after three runs, the Ag_3PO_4 nanoparticles can be concluded to be stable during the photocatalytic reaction.

Notably, the photocatalytic activity of Ag_3PO_4-120 is higher than that of Ag_3PO_4-P and N-TiO_2, which can be explained from the PL analysis. The PL spectra are widely used to investigate the migration, transfer, and recombination processes of the photogenerated electron-hole pairs in a semiconductor, since PL emission arises from the recombination of free carriers. Figure 9 shows the PL spectra of Ag_3PO_4-120, Ag_3PO_4-P, and N-TiO_2 excited by 254 nm. As shown in Figure 9, it is clear to see that there is a significant decrease in the PL intensity of Ag_3PO_4-120 compared to that of Ag_3PO_4-P and N-TiO_2. A weaker intensity of the peak represents a

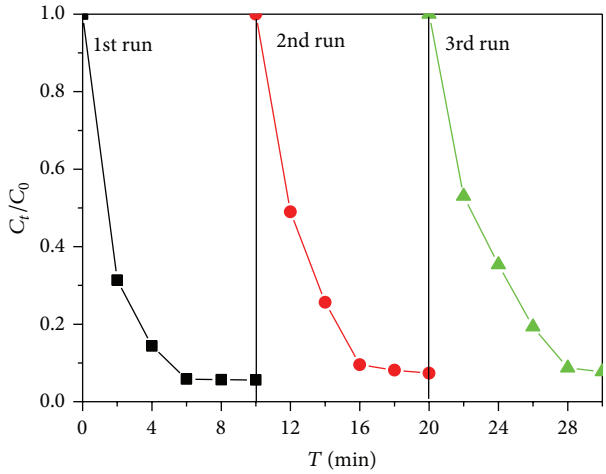

FIGURE 8: Degradation curves of MB with Ag_3PO_4-120 obtained by hydrothermal method for 3 cycles.

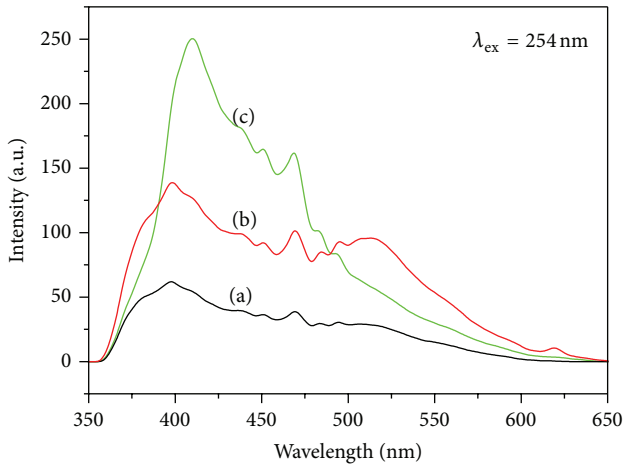

FIGURE 9: PL spectra of the as-synthesized samples: (a) Ag_3PO_4-120; (b) Ag_3PO_4-P; (c) N-TiO_2.

lower recombination probability of photogenerated charge carriers. The lower of the observed PL intensity can be associated with the electron transfer process from excited CB to VB in Ag_3PO_4 lattice, through which the process of electron transfer takes place. Hence, the samples prepared by this method prevent the charge carrier recombination probabilities and improve the separation of charge carriers. The decrease in intensity can also be attributed to the generation of new defect or vacancy sites like oxide ion vacancy [22]. Therefore, Ag_3PO_4-120 could effectively inhibit the recombination of photogenerated charge carriers, which helps the separation of photogenerated electron-hole pairs. It can be established that Ag_3PO_4-120 is very promising for the photocatalysis with satisfying efficiency.

4. Conclusion

In summary, we have demonstrated a facile and efficient hydrothermal method for fabricating Ag_3PO_4 submicron particles at low temperature. Moreover, its photocatalytic performance studies indicated that this novel Ag_3PO_4 structures exhibited much higher activities than that of Ag_3PO_4-P and N-doped TiO_2 for the organic contaminant degradation under visible light irradiation. This study clearly reveals that the rational fabrication of semiconductor nanostructure may be an effective technique for the development of highly efficient visible light sensitive photocatalysts.

Conflict of Interests

The authors declare that there is no conflict of interests regarding the publication of this paper.

Acknowledgments

The authors thank Youth Project of Yulin Normal University (2012YJQN03), National Natural Science Foundation of China (NSFC) (21363027), Guangdong Natural Science Foundation (S2013040013755), Colleges and Universities in Guangdong Province Science and Technology Innovation Project (2013KJCX0123), the Scientific Research Foundation of Guangxi University (XGZ130765), and Guangxi Key Science and Technology Program (2012AA07043).

References

[1] A. Fujishima and K. Honda, "Electrochemical photolysis of water at a semiconductor electrode," *Nature*, vol. 238, no. 5358, pp. 37–38, 1972.

[2] M. A. Fox and M. T. Dulay, "Heterogeneous photocatalysis," *Chemical Reviews*, vol. 93, no. 1, pp. 341–357, 1993.

[3] J. Tang, Z. Zou, and J. Ye, "Efficient photocatalytic decomposition of organic contaminants over $CaBi_2O_4$ under visible-light irradiation," *Angewandte Chemie International Edition*, vol. 43, no. 34, pp. 4463–4466, 2004.

[4] W. Yao, C. Huango, and J. Ye, "Hydrogen production and characterization of $MLaSrNb_2NiO_9$ (M = Na, Cs, H) based photocatalysts," *Chemistry of Materials*, vol. 22, no. 3, pp. 1107–1113, 2010.

[5] K. Maeda, K. Teramura, D. Lu, N. Saito, Y. Inoue, and K. Domen, "Noble-metal/Cr_2O_3 core/shell nanoparticles as a cocatalyst for photocatalytic overall water splitting," *Angewandte Chemie International Edition*, vol. 45, no. 46, pp. 7806–7809, 2006.

[6] S. Wang, L. Yi, J. E. Halpert et al., "A novel and highly efficient photocatalyst based on P_{25}- graphdiyne nanocomposite," *Small*, vol. 8, no. 2, pp. 265–271, 2012.

[7] T. Guohui, F. Honggang, J. Liqiang, X. Baifu, and P. Kai, "Preparation and characterization of stable biphase TiO_2 photocatalyst with high crystallinity, large surface area, and enhanced photoactivity," *The Journal of Physical Chemistry C*, vol. 112, no. 8, pp. 3083–3089, 2008.

[8] Y. Lai, M. Meng, Y. Yu, X. Wang, and T. Ding, "Photoluminescence and photocatalysis of the flower-like nano-ZnO photocatalysts prepared by a facile hydrothermal method with or without ultrasonic assistance," *Applied Catalysis B: Environmental*, vol. 105, no. 3-4, pp. 335–345, 2011.

[9] D. Ingram and S. Linic, "Water splitting on composite plasmonic-metal/semiconductor photoelectrodes: evidence for selective plasmon-induced formation of charge carriers near the

semiconductor surface," *Journal of the American Chemical Society*, vol. 133, no. 14, pp. 5202–5205, 2011.

[10] P. Wang, B. B. Huang, X. Y. Qin et al., "Ag@AgCl: ahighly efficient and stable photocatalystactive under visible light," *Angewandte Chemie International Edition*, vol. 47, no. 41, pp. 7931–7933, 2008.

[11] G.-F. Huang, Z.-L. Ma, W.-Q. Huang et al., "Ag_3PO_4 semiconductor photocatalyst: possibilities and challenges," *Journal of Nanomaterials*, vol. 2013, Article ID 371356, 8 pages, 2013.

[12] Z. Yi, J. Ye, N. Kikugawa et al., "An orthophosphate semiconductor with photooxidation properties under visible-light irradiation," *Nature Materials*, vol. 9, no. 7, pp. 559–564, 2010.

[13] Y. Bi, S. Ouyang, J. Cao, and J. Ye, "Facile synthesis of rhombic dodecahedral AgX/Ag_3PO_4 (X = Cl, Br, I) heterocrystals with enhanced photocatalytic properties and stabilities," *Physical Chemistry Chemical Physics*, vol. 13, no. 21, pp. 10071–10075, 2011.

[14] Y. P. Bi, S. Ouyang, N. Umezawa, J. Cao, and J. Ye, "Facet effect of single-crystalline Ag_3PO_4 sub-microcrystals on photocatalytic properties," *Journal of the American Chemical Society*, vol. 133, no. 17, pp. 6490–6492, 2011.

[15] X. S. Zhou, B. Jin, L. D. Li et al., "A carbon nitride/TiO_2 nanotube array heterojunction visible-light photocatalyst: synthesis, characterization, and photoelectrochemical properties," *Journal of Materials Chemistry*, vol. 22, no. 34, pp. 17900–17905, 2012.

[16] X. Zhou, F. Yang, B. Jin, L. Chen, and S. Li, "Fabrication of CdS/H-TiO_2 nanotube arrays and their application for the degradation of methyl orange in aqueous solutions," *Journal of Nanomaterials*, vol. 2014, Article ID 678505, 7 pages, 2014.

[17] C.-T. Dinh, T.-D. Nguyen, F. Kleitz, and T.-O. Do, "Large-scale synthesis of uniform silver orthophosphate colloidal nanocrystals exhibiting high visible light photocatalytic activity," *Chemical Communications*, vol. 47, no. 27, pp. 7797–7799, 2011.

[18] M. Li, S. K. Cushing, Q. Wang et al., "Size-dependent energy transfer between CdSe/ZnS quantum dots and gold nanoparticles," *The Journal of Physical Chemistry Letters*, vol. 2, no. 17, pp. 2125–2129, 2011.

[19] R. Vinu and G. Madras, "Photocatalytic activity of Ag-substituted and impregnated nano-TiO_2," *Applied Catalysis A: General*, vol. 366, no. 1, pp. 130–140, 2009.

[20] Y. Yu and J. Zhang, "Ultrafast electrodeposition of amorphous carbon nitride films from fullerene derivative," *Electrochemistry Communications*, vol. 12, no. 3, pp. 390–393, 2010.

[21] M. J. Bierman and S. Jin, "Potential applications of hierarchical branching nanowires in solar energy conversion," *Energy & Environmental Science*, vol. 2, no. 10, pp. 1050–1059, 2009.

[22] L. Yang, Y. Zhang, W. Ruan, B. Zhao, W. Xu, and J. R. Lombardi, "Improved surface-enhanced Raman scattering properties of TiO_2 nanoparticles by Zn dopant," *Journal of Raman Spectroscopy*, vol. 41, no. 7, pp. 721–726, 2010.